GAMBIT Database and Explorer
for Real-Time IRI Maps of F2 Layer Peak Height and Density

I. A. Galkin[1], A. M. Vesnin[1], X. Huang[2], A.V. Kozlov[1], P. Song[1], and B. W. Reinisch[1,2]

[1] University of Massachusetts Lowell, Space Science Laboratory
600 Suffolk Street, Lowell, MA 01854 USA, Tel: +1 978-934-4912, Fax: +1 978-459-7915
[2] Lowell Digisonde International, LLC, Lowell, MA 01854, USA

ABSTRACT

The Global Ionosphere Radio Observatory (GIRO) ingests ionosonde data (foF2, hmF2, etc.) in databases at the Lowell GIRO Data Center (LGDC). Every 15 minutes when new data arrive, the IRI-based Real-Time Assimilative Mapping (IRTAM) algorithm at LGDC generates real-time maps of foF2 and hmF2. The IRTAM morphs the empirical "climatology" IRI model into agreement with the GIRO measurements, so that the new model representations of the ionosphere closely follow its "weather" variability. The new "GAMBIT" database (Global Assimilative Modeling of Bottomside Ionospheric Timelines) at LGDC now offers a unique Internet-accessible data resource for the timeline of the revised foF2 and hmF2 maps. GAMBIT makes these maps available for visualization and user applications in the compact form of expansion coefficients. The GAMBIT explorer also offers a suite of tools for inspection/validation of the IRTAM results by comparisons with coincident global GNSS TEC maps acquired from the MIT Madrigal repository. Initial results of the statistical IRTAM validation are presented using 13+ million records in GAMBIT collected over a 15–year period from 2000 to 2015. Using the GAMBIT database we test the performance of IRTAM during well documented space weather events like the interplanetary shock and the subsequent storm of 7-8 November 2004. The conducted analysis sheds lights on the capabilities of the IRTAM technologies to describe global ionospheric timelines and reveals their potential to predict system dynamics over no-data areas (spatial interpolation) and in time (short-term forecast).

1. INTRODUCTION

"Space weather" as a discipline has been following the successful path of its terrestrial counterpart with implementations of the recursive Kalman filter in the framework of a theoretical "first-principles" model of the system. During the update step of the Kalman filter, the underlying model is brought into agreement with observations by manipulating the model drivers, thus not only gleaning the system nowcast from the fragmentary observations, but also producing a self-consistent physics-based description of the multiple processes that constitute the system. During the forecast step of the Kalman filter, thus updated theoretical model is promoted one step into the future, forming the starting point for the next update step computations.

However, the physics-based Kalman filter, highly successful in meteorological applications, has been facing significant challenges in its implementation for the space weather domain [*McNamara, et al.,* 2008], which is known for its complexity of dynamically coupled constituent systems (Sun, interplanetary space, magnetosphere, plasmasphere, ionosphere, and atmosphere), sensitivity to external drivers in the Sun-Earth realm, uncertainty of the sensor measurements because of inherent noise and biases, and ultimately, scarceness of observations useable for timely space weather reports. While these challenges are being addressed [*Schunk, et al.,* 2014], simpler model architectures are investigated for the task of nowcasting the Earth's near space conditions, in particular those based on

1

the assimilative extensions to the International Reference Ionosphere (IRI) [*Bilitza, et al.,* 2011], an empirical model of ionospheric climatology.

The empirical models capture the average essence of the observed system behavior by representing historical data as a compact set of expansion coefficients into a suitable functional basis, for example spherical or diurnal harmonics. Once the coefficients are computed from the available observations (the model is trained), the result can be used to predict the average system state for any given time and space. In one of the proposed assimilative extensions for IRI [*Galkin, et al.,* 2012], such trained empirical model is used as the underlying model at the update step so that its corrected formulation can closely follow the timeline of the system dynamics. At each update step, the empirical model formalism is kept unchanged and the original coefficients of expansion are merely adjusted to minimize differences between observations and model. Such model-morphing technique preserves the characteristic features of the ionospheric plasma distributions captured during the training phase.

The empirical and physics-based approaches are in fact complementary: the physics-based assimilation sheds light on the system state in terms of the multiple ongoing coupled processes that are responsible for the model outcome, while the empirical assimilation is capable of representing events that are yet to be understood and described theoretically. Contrasting two types of models applied to the same sensor data is a powerful means to explore unknown dynamics of the ionosphere.

2. IRI-BASED REAL-TIME ASSIMILATIVE MODEL

The IRI-based Real-Time Assimilative Model (IRTAM) uses observational data from the Global Ionosphere Radio Observatory (GIRO) [*Reinisch and Galkin,* 2011] that are available at the Lowell GIRO Data Center (LGDC) within a few minutes from their registration. As of April 2015, up to 45 ionosondes, mostly Digisondes® [*Reinisch et al.,* 2009], are sending in near real time ionogram-derived records for assimilation to LGDC. IRTAM publishes the resulting assimilative maps of the F2 layer critical frequency foF2 and peak height hmF2 every 15 minutes at http://giro.uml.edu/IRTAM/ for immediate visualization (Figure 1).
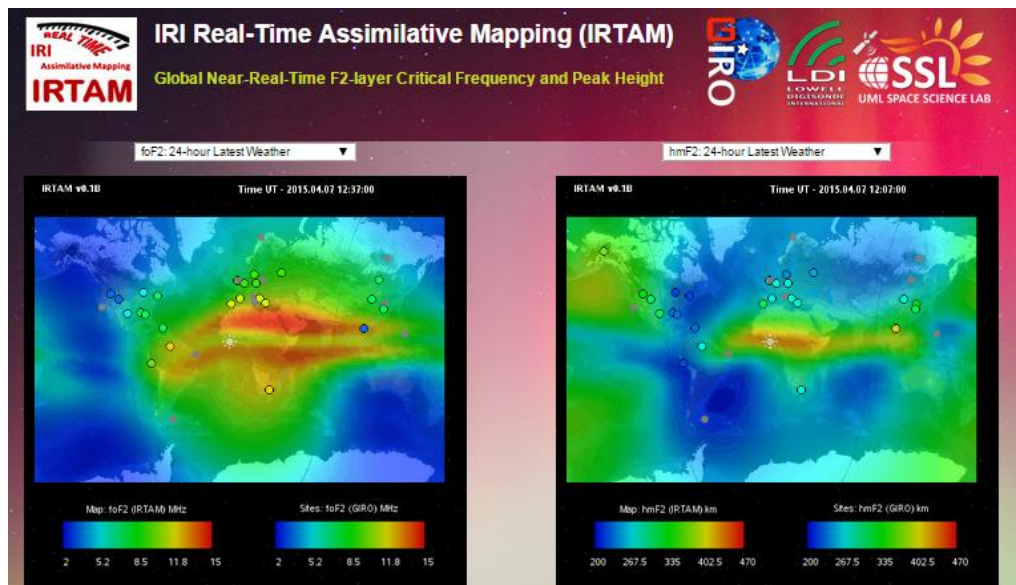
Figure 1. Real-time global maps of foF2 (left) and hmF2 (right) produced and published by IRTAM at http://giro.uml.edu/IRTAM. Dots depict the GIRO ionosondes contributing data to IRTAM.

The IRTAM is a 4D Data Assimilation (4DDA) algorithm [Galkin *et al.,* 2012] whose update step involves substantially long periods of past observations (rather than only the latest system state snapshot as in 3DDA computations). Even 4DDA algorithms that look at only 1-2 update steps back have proven superior to 3DDA, though at substantial computational expense. For IRTAM, relative simplicity of the underlying model formalism in comparison to the physics-based models has allowed 4DDA computations to span past history of model-vs-observation behavior for up to 24 hours. The capability to involve a large context of the temporal analysis has strengthened multiple aspects of operations, including robustness to data artifacts (gaps, errors) and spatial prediction of LT-bound processes, as further discussed below.

2.1 INTERPOLATION THROUGH DATA GAPS AND ERRORS

In the model-morphing approach to assimilation, the outcome of the update step is no longer a computation of the physics-based model driven by the optimal set of driving parameters; instead it is an expansion to a functional basis that minimizes the observation-model differences. As such, the morphing procedure is prone to the usual weaknesses of expansion over no-data areas in time and space, where unconstrained expansion can produce totally unreasonable, and in particular oscillating representations of the missing data. Introduction of phantom points that constrain the expansion is one possibility of avoiding such problems, as employed by *Jones and Gallet* [1962] in their original development of the CCIR maps for the F2-layer critical frequency foF2 used in IRI. Ensuring that the morphing process is *elastic* is another option that we have introduced to avoid unreasonable expansion.
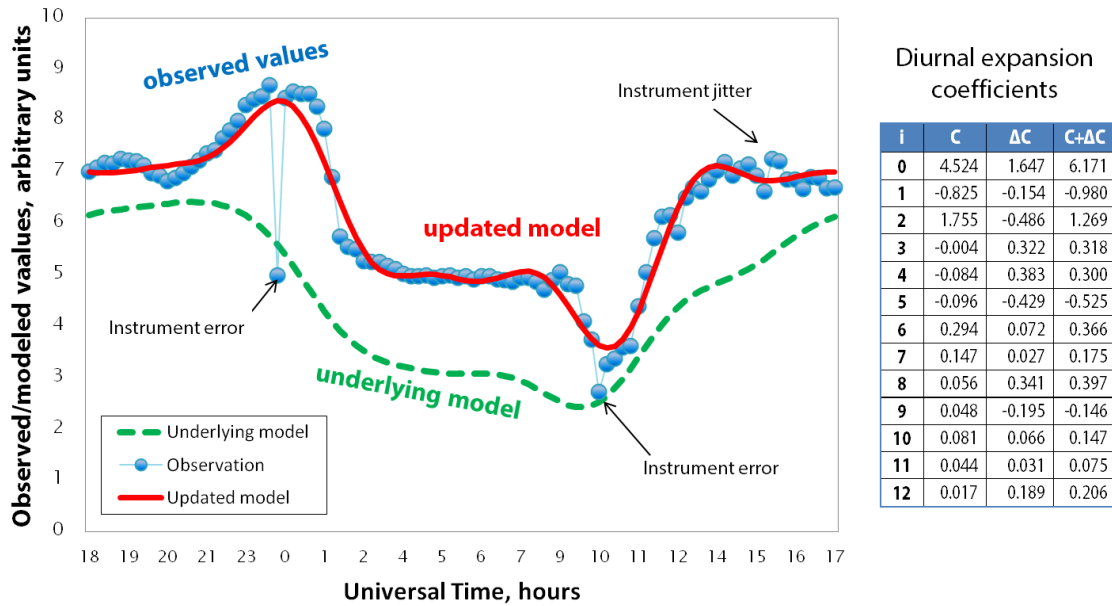
Adding phantom points to the observational data in order to constrain the expansion process is a common, though controversial approach. We avoid much of the "interpolation" criticism by first analyzing the time series of differences between observation and model at each sensor location. Here the interpolation is not required, unless data are missing due to an instrument malfunction or a geospace anomaly. We take a day's worth of observations and easily compute diurnal harmonics of the $\Delta V = V_{obs}\text{-}V_{mod}$, where V_{obs} are observed and V_{mod} are model values:

$$\Delta V = \Delta C_0 + \sum_{i=1}^{N} \Delta C_{2i-1} \cos i\tau + \Delta C_{2i} \sin i\tau \tag{1}$$

Here the ΔC_i are expansion coefficients, N is the order of diurnal expansion, and τ is time of day expressed as diurnal phase in degrees, ($-180° \leq \tau \leq 180°$). The order N determines the minimum scale of time dynamics that will be resolved by this expansion; in practice, its selection is driven by the amount of input data jitter and errors caused by acquisition and processing. Reasonable values of N between 6 and 12 (corresponding to the minimum resolved time scale of 4 to 2 hours) result in the number of computed ΔC_i coefficients ranging from 13 to 25; such expansion task is over-determined and easily arranged at observation cadences of 30 minutes or better.

Figure 2 presents an example of such a "single-site" computation, in which the time series of observed V_{obs} (blue circles) and model V_{mod} (green dashed line) values are processed to derive a new set of coefficients $C^*=C+\Delta C$, where C are the original coefficients of the trained model, and compute the resulting updated model V_{up} (red line) using

$$V_{up} = C_0^* + \sum_{i=1}^{N} C_{2i-1}^* \cos i\tau + C_{2i}^* \sin i\tau \tag{2}$$

| i	C	ΔC	C+ΔC
0	4.524	1.647	6.171
1	-0.825	-0.154	-0.980
2	1.755	-0.486	1.269
3	-0.004	0.322	0.318
4	-0.084	0.383	0.300
5	-0.096	-0.429	-0.525
6	0.294	0.072	0.366
7	0.147	0.027	0.175
8	0.056	0.341	0.397
9	0.048	-0.195	-0.146
10	0.081	0.066	0.147
11	0.044	0.031	0.075
12	0.017	0.189	0.206

Figure 2. Single-location assimilation of time-domain data by correcting coefficients of the diurnal harmonic expansion. Differences between observed values (dots) and the underlying model (dashed line) are used to compute correction coefficients ΔC that are then applied to the original coefficients C_i to obtain the updated model (solid line).

If the sensor instrument is capable of continuous error-free data acquisition and processing, the computation of ΔC presents no difficulty. In practice, however, this is rarely the case; gaps and erroneous values are common with many types of remote sensing equipment that require post-analysis for derivation of the data for assimilation. As seen in Fig. 2, the update operation is immune to occasional instrument mishaps and jitter caused by interference that reduces data quality. This protection is one of the strong benefits of using the 4DDA scheme with a large time window of prior data. The single-site technique, however, cannot intelligently handle the instrumental bias: it faithfully represents it by adjusting ΔC_0. Compensating biases is postponed till the spatial analysis phase of the assimilation.

## 2.2 SPATIAL INTERPOLATION OF LONG-TERM LT-BOUND PROCESSES

The 24-hour context of the 4DDA analysis in IRTAM is responsible for an intriguing capability to spatially predict certain aspects of the ionospheric behavior outside the GIRO coverage, Figure 3 illustrates this capability. The left panel shows the difference foF2 map (IRTAM minus IRI) for 2012.10.17 18:30 UT when no data from South Africa were ingested. The right panel shows the corresponding map when the South Africa data are included in the IRTAM calculation; note the significant density enhancement over South Africa. Interestingly, the left panel also indicates an enhanced electron density over the West Coast of Africa even though the South Africa data were not used. The detected effect is a result of the spatial extrapolation qualities of the IRTAM that can detect LT-bound behavior of foF2 in 24-hour data. As the GIRO sensors rotate with the Earth, the long-term harmonics of the ensemble of foF2 deviations from the IRI prediction are identified in the individual station data and extrapolated to the neighboring longitudes.

4
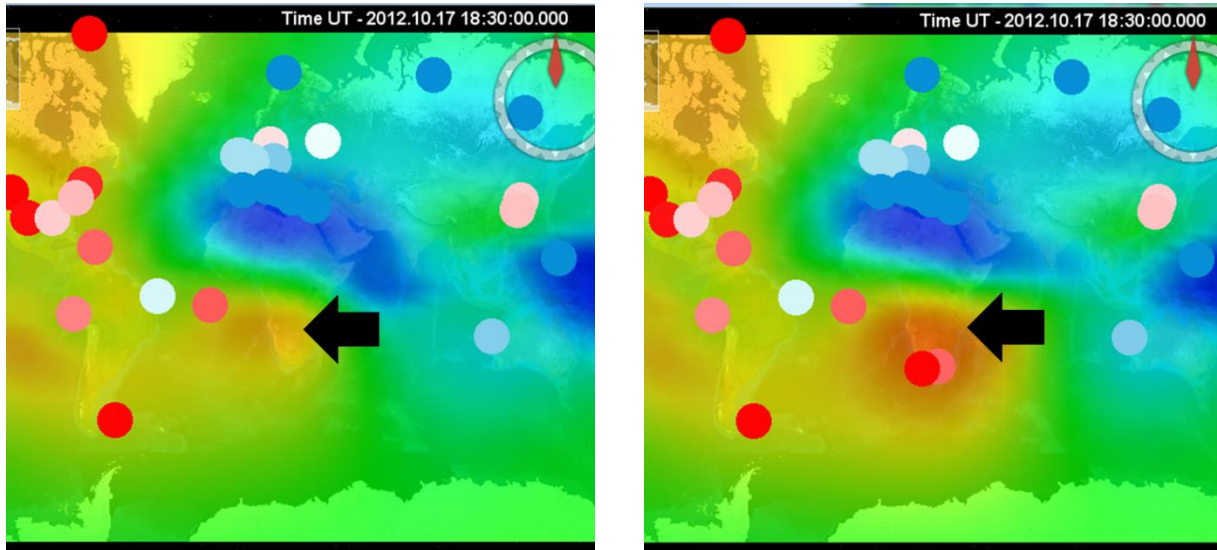
Figure 3. Difference maps of foF2 (IRTAM assimilation minus IRI climatology) at 2012.10.17 18:30 UT showing deviation of observed ionospheric plasma density from predicted behavior. Left: no SA data, arrow points to a slight increase of foF2 over the African West Coast. Right: with SA data, strong enhancement of foF2 over Africa.

3. GAMBIT DATABASE AND EXPLORER

Primary objective for GAMBIT Explorer (Figure 4) is to provide an interactive open analysis environment for IRTAM with rapid data visualization and validation.
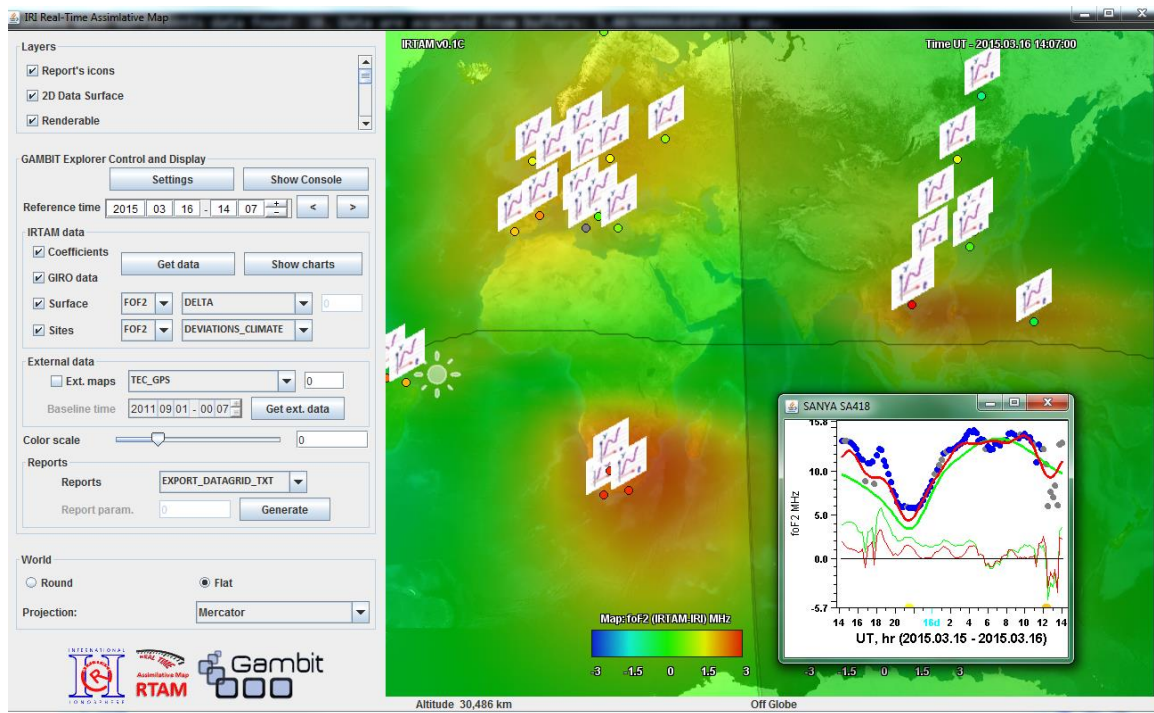

Figure 4. GAMBIT Explorer software mated to LGDC-operated GAMBIT Database for access, visualization, download, and export of global foF2 and hmF2 maps computed by IRTAM. GAMBIT Explorer is an open-source project maintained at git.giro.uml.edu.

The GAMBIT Explorer software is written in Java with NASA WorldWind graphics library for multi-platform operations; it is maintained under the open source license [http://git.giro.uml.edu] and available for installation at GAMBIT homepage [http://giro.uml.edu/GAMBIT].

3.1 VALIDATING IRTAM WITH GPS TEC MAPS

The new GAMBIT Explorer tool supports comparative analysis of the IRTAM foF2 and hmF2 maps and the GPS TEC maps acquired from the Open Madrigal node at MIT Haystack Observatory [*Rideout and Coster,* 2006]. Three panels of Fig.5 illustrate views of the same substorm event on March 17, 2015 at 23:22UT with the left panel showing deviations of GPS TEC from the reference values observed one day earlier at the same UT time, the middle panel – deviation of IRTAM's foF2 from the IRI prediction, and the right panel – deviation of IRTAM's hmF2 from the IRI prediction. The superiority of the spatial coverage and resolution of the GPS data (thousands versus tens of sensors) becomes evident in this comparison; the remarkable super-fountain effect in the American sector during this storm phase is underrepresented in the IRTAM foF2 map because of the poor GIRO coverage in north-western South America. Interesting is that the strong negative effect in the peak density shown by IRTAM over North America is not seen in the TEC data, suggesting a vertical restructuring of the plasma due to an upflow of plasma. The dynamics of the ionospheric peak escapes the evaluation in GPS data.

TEC Deviation	foF2 Deviation	hmF2 Deviation
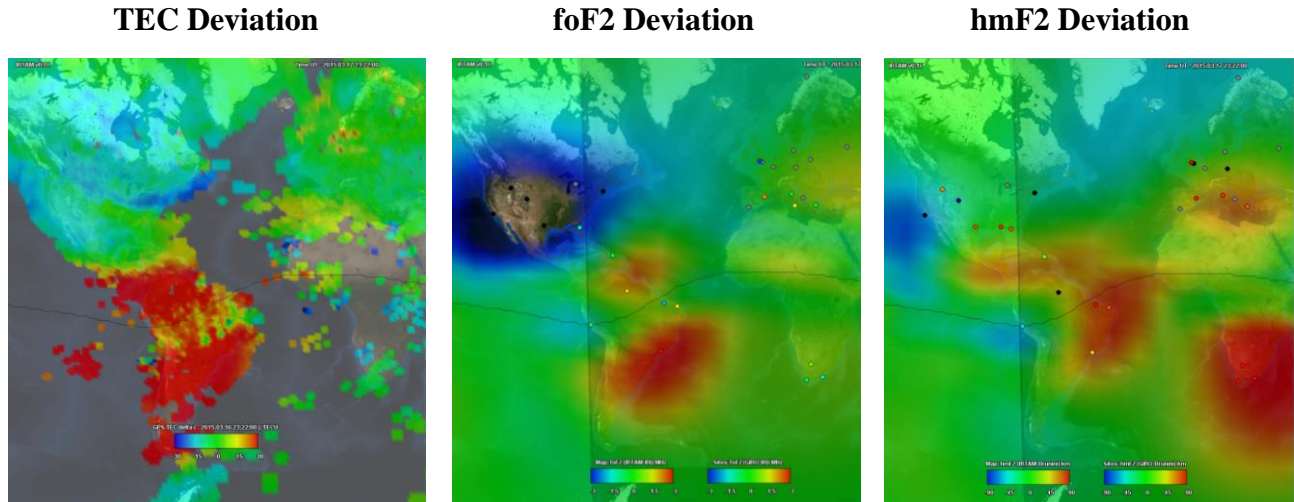
Figure 5. The early phase of the March 2015 substorm at 23:22UT on March 17 as seen in GPS TEC (left), and IRTAM foF2 (middle) and hmF2 (right)

3.2 VALIDATING IRTAM TIMELINES DURING MAJOR GEOSPACE EVENTS

Frame-by-frame inspection of the global differential foF2 and hmF2 maps in GAMBIT is a convenient tool for validating IRTAM representation of major geospace events. The differential maps provide rapid insight in deviations of the ionospheric dynamics from their expected climatological behavior. As a case study, we looked at IRTAM computations during the November 7-11, 2004, a time period characterized by several storm activities, including an interplanetary shock event on November 7 and subsequent plasmaspheric refilling studied by multiple research teams. The objective of the IRTAM validation was to ensure that IRTAM results are in agreement with the interpretations provided by other researchers and inspect IRTAM timelines for signatures overlooked in analysis.
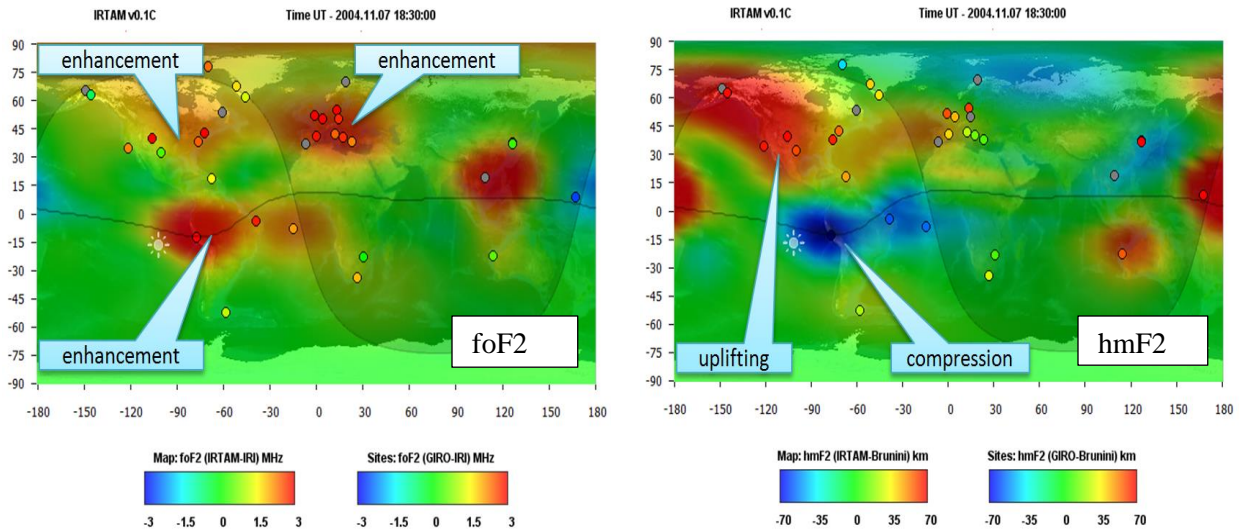
Figure 6. Ionospheric effects of the interplanetary shock passage at 1830 UT on 7 November 2004 as seen in ΔfoF2 (left) and ΔhmF2 (right) IRTAM maps. Maps are calculated for the moment immediately after the shock impact on the Earth's magnetosphere.

In Fig.6, the ionospheric effects at 18:30 UT from the IP shock arrival as seen by IRTAM are labeled; with the daytime equatorial compression (northward Bz) being the signature shock effect reported previously [e.g., *Zong, et al.,* 2010]. The compression manifests itself in the IRTAM maps as combined hmF2 drop and foF2 enhancement. Incidental nighttime density enhancements over Europe and Asia, as well as apparent plasma uplift in Northern American sector eluded attention in the literature. In part, an extraordinary ionospheric activity during the first half of November 2004 is responsible for difficulties in traditional day-to-day comparative analysis: none of the days around November 7, 2004 could serve as a good quiet-time reference. In fact, majority of the IRTAM differential maps during those days showed a multitude of anomalies, so that selecting the IRI long-term prediction as the reference for their study is a sensible approach.
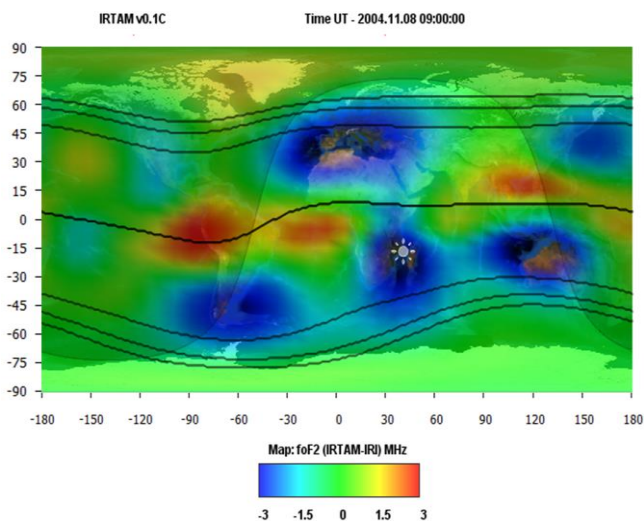
Figure 7. Plasmasphere refilling seen in *ΔfoF2* map on November 8, 2004 09:00 UT. L-shells surface projections are given at L= 2, 3, and 4.

Following the November 7, 2004 IP shock event, a strong ionospheric effect persisted for over 12 hours, clearly visible in the IRTAM maps as a combination of density depletion off the Appleton anomaly up to mid-latitudes and density enhancement along the magnetic equator (Fig. 7), attributed to ongoing process of the plasmasphere refilling. Coincident observation of the plasmaspheric densities by the IMAGE Radio Plasma Imager [*Reinisch, et al.,* 2004] confirm this interpretation. Apparently, during the recovery phase of the storm, relatively empty flux tubes of the plasmasphere cause an enhanced plasma outflow from the ionosphere on the day side. Lesser nightside effect is likely to be due to smaller ratio of the densities in plasmasphere and ionosphere;

however, the effect is still pronounced in comparison to the expected plasma flow in the opposite direction from the plasmasphere to the ionosphere.

4. SUMMARY AND OUTLOOK
Newly introduced GAMBIT Database and Explorer environment, with the access portal at http://giro.uml.edu/GAMBIT/, allows rapid access to 15-minute timelines of the global maps of ionospheric peak height and density calculated by an assimilative model IRTAM, including the near real-time computations. Increased access activity to detailed GAMBIT timelines suggests that their utility as a space weather resource is recognized. To help further integration of GAMBIT in variety of academic applications, the GAMBIT is adopting open source model of development. Studies of the ionospheric timelines through the most interesting events in the Sun-Earth environment will bring new insights in their progression and potential for increased accuracy of their forecast.

ACKNOWLEDGEMENTS

REFERENCES

Bilitza, D., L.-A. McKinnell, B.W. Reinisch, and T. Fuller-Rowell (2011), The international reference ionosphere today and in the future, *Journal of Geodesy*, doi:10.1007/s00190-010-0427-x.

Galkin, I. A., B. W. Reinisch, X. Huang, and D. Bilitza (2012), Assimilation of GIRO Data into a Real-Time IRI, *Radio Sci.,* 47, RS0L07, doi:10.1029/2011RS004952.

Jones, W.B., R.M. Gallet (1962), Representation of diurnal and geographical variations of ionospheric data by numerical methods. *ITU Telecommun. J.* 29 (5), 129–149, 1962.

McNamara L.F., C.R. Baker, and D.T. Decker (2008) Accuracy of USU-GAIM specifications of foF2 and M(3000)F2 for a worldwide distribution of ionosonde locations, *Radio Science,* 43(1). doi:10.1029/2007RS003754.

Reinisch, B. W., X. Huang, P. Song, J. L. Green, S. F. Fung, V. M. Vasyliunas, D. L.Gallagher, and B. R.Sandel (2004), Plasmaspheric mass loss and refilling as a result of a magnetic storm*, J. Geophys. Res., 109*(A1), A01202, doi:10.1029/2003JA009948.

Reinisch, B.W., I.A. Galkin, G.M. Khmyrov, et al. (2009), The New Digisonde for Research and Monitoring Applications, *Radio Sci*., *44* RS0A24, doi:10.1029/2008RS004115.

Reinisch, B.W. and I.A. Galkin (2011), Global Ionospheric Radio Observatory (GIRO), *Earth Planets Space*, vol. 63 no. 4 pp. 377-381, doi:10.5047/eps.2011.03.001.

Rideout, W. and A. Coster, Automated GPS processing for global total electron content data (2006), *GPS Solutions*, 10.3, doi: 10.1007/s10291-006-0029-5.

Schunk, R.W., M. David, V. Eccles, L.C. Gardner, and L. Zhu (2014), Studies to Improve the Science in the GAIM - Full Physics Model, *N00014-09-1-0292 Final Report,* Utah State University, Logan, UT. Retrieved on March 12, 2015 from http://www.dtic.mil/cgi-bin/GetTRDoc?Location=U2&doc=GetTRDoc.pdf&AD=ADA603956

Zong, Q.-G., B. W. Reinisch, P. Song, Y. Wei, and I. Galkin (2010), Dayside ionospheric response to the intense interplanetary shocks/solar wind discontinuities: Observations from the digisonde global ionospheric radio observatory, *J. Geophys. Res.*, *115*, A06304, doi:10.1029/2009JA014796,